Int. J. Solids Structures Vol. 25, No. 10, pp. 1143–1156, 1989
Printed in Great Britain.

0020–7683/89 $3.00 + .00
© 1989 Pergamon Press plc

NUMERICAL STUDY OF LOCALIZATION IN A VOID-SHEET

VIGGO TVERGAARD
Department of Solid Mechanics, The Technical University of Denmark, Bldg. 404, DK-2800, Lyngby, Denmark

(*Received* 20 *September* 1988)

Abstract—A single layer of voids in a ductile solid, with no other voids present, acts as an inhomogeneity that promotes the onset of plastic flow localization in a shear band. For such a void-sheet consisting of a row of circular cylindrical voids the onset of localization is analysed, taking full account of the interaction between neighbouring voids. If a porous ductile material model is used to analyse this behaviour, representing the void-sheet as a slice of material with initial porosity, the void volume fraction to be used is not well defined. However, the present full numerical analysis of the localization problem is used to calibrate the simple model. Also the effect of inclusions inside nucleated voids is studied, and it is found that the additional void growth enforced by such inclusions can have a significant influence on localization predictions.

1. INTRODUCTION

Several investigations of ductile materials containing microscopic voids have shown that the resistance to localization of plastic flow in a shear band is strongly influenced by porosity. Yamamoto (1978) made use of Gurson's (1977) dilatant plasticity model of a porous ductile solid to show this dependence, and the effect of void nucleation was included in studies based on the same material model by Needleman and Rice (1978) and Saje *et al.* (1982). More recent studies have shown that the additional influence of the formation of a rounded corner on the yield surface, modelled in terms of a kinematic hardening description of a porous ductile material, results in earlier localization (Mear and Hutchinson, 1985; Tvergaard, 1987).

Cell model studies representing the effect of periodic arrays of voids have also been used to directly study the onset of localization in ductile porous solids. Such studies take full account of the nonuniform stress and strain distributions and the interaction between neighbouring voids, whereas the porous ductile material models represent the local stress distribution around voids in terms of an average flow stress value. For a square array of circular cylindrical voids in a material subject to plane strain tension Tvergaard (1981) has analysed the bifurcation into a periodic pattern, which represents the mode of deformation inside a shear band. It was found that after a small modification of the Gurson model, localization predictions based on this model were in good agreement with those obtained by the more accurate numerical study. This covers the critical values of strains and stresses as well as the angle of inclination of the first critical shear band.

Analyses for a circular cylindrical body containing a spherical void have been used by Tvergaard (1982) to investigate a material with a periodic distribution of spherical voids. This cell model was also used to predict localization, but due to the assumption of axisymmetry only bands normal to the maximum principal tensile stress can be represented. More recently, the same type of model problem has been used by Koplik and Needleman (1987) to study the void coalescence behaviour well beyond the onset of localization. In order to consider localization in an inclined shear band for a material containing spherical voids a full three-dimensional analysis is required, as that carried out recently in a study of the interaction of two size-scales of voids (Tvergaard, 1988).

If the voids are only present along a single plane in the material, this void sheet will act as an imperfection, which promotes localization along that plane. In terms of a porous material model this situation would be represented by a thin slice of material containing initial porosity, with no porosity outside. However, the void volume fraction to be used

inside the band is not well defined when there is only a single layer of voids. With this quantity undefined, a cell model study is needed to determine the localization behaviour, taking into account the actual stress and strain fields in the material near the voids. Such analyses are carried out here for a layer of circular cylindrical voids in a material subject to plane strain conditions.

The problem considered here is also of interest in other cases where voids tend to appear in a single layer. Thus, in an aluminum alloy with coarse grain boundary particles, investigated by Becker *et al.* (1989), voids nucleate at the grain boundaries, and the appropriate width of the grain boundary porous zone is an issue, as well as the appropriate void volume fraction inside this zone.

2. PROBLEM FORMULATION

In the material analysed the initial inhomogeneity is represented by a row of uniformly spaced circular cylindrical holes with the radius R_0 and the spacing $2D_0$, as shown in Fig. 1. The initial angle of inclination between the void-sheet and the x^1-axis is ψ_0. The dimensions of the block of material are assumed infinite relative to the void spacing, and the principal macroscopic true stresses are σ_1 and σ_2 in the x^1- and x^2-directions, respectively. Thus, the material far from the void sheet must behave as a uniformly strained material subject to the prescribed stress history. All significant differences from this uniform field are contained in a band around the voids, as that between the two dashed lines parallel with the void sheet in Fig. 1. If the band is made sufficiently wide relative to the void spacing, the fields in the outer parts of the band will be essentially identical to the uniform fields outside the band.

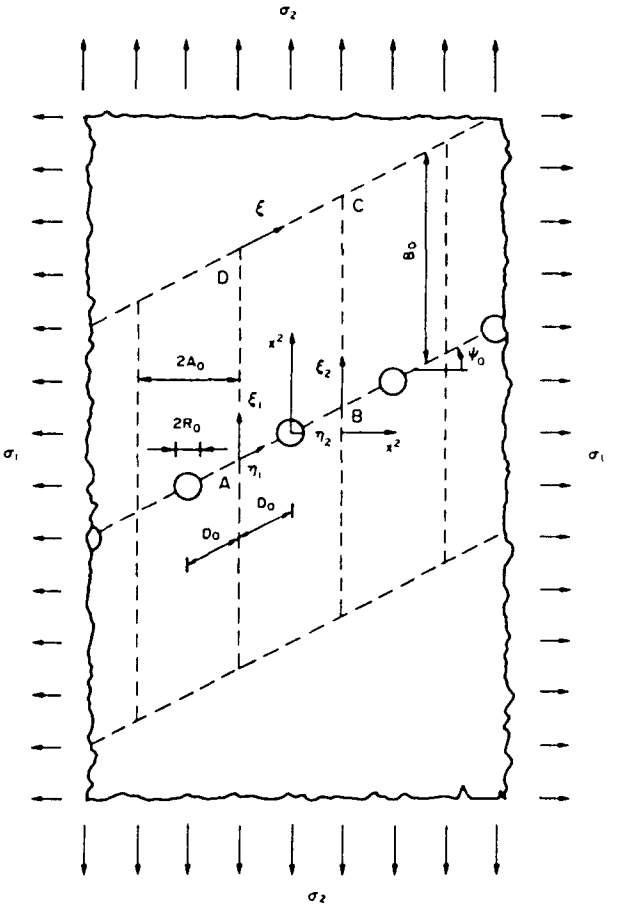

Fig. 1. Material containing a row of uniformly spaced circular cylindrical voids. The region ABCD is analysed numerically.

As shown in Fig. 1 the band is divided into a number of cells with sides parallel to the x^2-axis. The initial width of a cell is $2A_0 = 2D_0 \cos \psi_0$ and the initial height is B_0, so that the initial width of the band analysed is $2B_0 \cos \psi_0$. Since the solution is periodic along the void sheet, with a period corresponding to the void spacing, all the cells undergo identical behaviour. Therefore, in the numerical solution it is only necessary to analyse one of the cells, i.e. the region ABCD shown in Fig. 1. The formulation of the boundary conditions for this cell is rather similar to that used by Fleck *et al.* (1988) in a study of the nucleation and growth of voids in a shear field. However, in the present shear localization problem the width of the cell changes and the edges rotate due to the straining of the far field. Thus, if the current principal logarithmic strains in the far field are ε_1 and ε_2 (in the x^1- and x^2-directions, respectively), the current width of the cell is controlled by ε_1 and the current angle of inclination ψ of the void sheet is given by

$$\tan \psi = e^{(\varepsilon_2 - \varepsilon_1)} \tan \psi_0. \tag{1}$$

The boundary conditions are specified in terms of the Cartesian displacement components u^i and the nominal traction components T^i, where $u^3 \equiv 0$ since plane strain conditions are considered. When it is assumed that the centre of the void belonging to the cell ABCD does not move, the displacement components u_A^i and u_B^i at the two corner points A and B are determined by the far field strains ε_1 and ε_2 and the rotation (1) as

$$u_B^1 = -u_A^1 = A_0(e^{\varepsilon_1} - 1) \tag{2}$$

$$u_B^2 = -u_A^2 = A_0(e^{\varepsilon_1} \tan \psi - \tan \psi_0). \tag{3}$$

Similar conditions apply to the edge DC, but here the displacements are also assumed to vary linearly between the two corners, to give complete compatibility with the far field. Thus, in terms of the length measuring coordinate ξ on DC the displacements are

$$u^1(\xi) = u_D^1 + \frac{\xi}{2D_0}(u_B^1 - u_A^1) \tag{4}$$

$$u^2(\xi) = u_D^2 + \frac{\xi}{2D_0}(u_B^2 - u_A^2). \tag{5}$$

Furthermore, the resultant forces on the edge DC must agree with the stress field outside the band

$$\int_0^{2D_0} T^2 \, d\xi = \sigma_2(2A_0 + u_B^1 - u_A^1) \tag{6}$$

$$\int_0^{2D_0} T^1 \, d\xi = -\sigma_1(2D_0 \sin \psi_0 + u_B^2 - u_A^2). \tag{7}$$

On the cell sides AD, BC and AB the periodicity and symmetry conditions are such that equilibrium and compatibility with the neighbouring cells is satisfied. This is expressed by using the length measuring coordinates ξ_1, ξ_2, η_1 and η_2 (see Fig. 1).

$$u^1(\xi_1) - u_A^1 = u^1(\xi_2) - u_B^1 \tag{8}$$

$$u^2(\xi_1) - u_A^2 = u^2(\xi_2) - u_B^2 \tag{9}$$

$$T^1(\xi_1) = -T^1(\xi_2), \qquad T^2(\xi_1) = -T^2(\xi_2) \tag{10}$$

$$u^1(\eta_1) = -u^1(\eta_2), \qquad u^2(\eta_1) = -u^2(\eta_2) \tag{11}$$

$$T^1(\eta_1) = T^1(\eta_2), \qquad T^2(\eta_1) = T^2(\eta_2). \tag{12}$$

The conditions at the void surface, $(x^1)^2+(x^2)^2 = R_0^2$, are

$$T^1 = T^2 = 0. \tag{13}$$

If there is a particle inside the void, the conditions are more complex, as has been discussed by Fleck *et al.* (1988). Then the conditions at the void surface are conveniently expressed in incremental form, where $\dot{(\ )}$ denotes a small increment, using the current angle ϕ between the x^1-axis and the surface point considered. For a bonded particle (13) is replaced by

$$\dot{u}^1 \cos\phi + \dot{u}^2 \sin\phi = 0, \qquad -\dot{u}^1 \sin\phi + \dot{u}^2 \cos\phi = R_0\dot{\theta}. \tag{14}$$

Here, $\dot{\theta}$ is the incremental angle of rotation of the particle, which is determined such that no resultant moment acts on the particle.

Void nucleation is modelled in a few computations by assuming that all points on the void surface are released from the surface simultaneously (see also Fleck *et al.*, 1988), while the surface tractions are stepped down to zero in a few subsequent increments. At points where the radius decreases below R_0, sliding contact with the particle is assumed, described by

$$\dot{u}^1 \cos\phi + \dot{u}^2 \sin\phi = 0, \qquad -\dot{T}^1 \sin\phi + \dot{T}^2 \cos\phi = 0. \tag{15}$$

This sliding contact remains as long as the normal stress is compressive, while other points of the void surface satisfy (13).

To summarize, equilibrium and compatibility inside the slice of material analysed is enforced by the edge conditions (8)–(15), together with the field equations inside the region ABCD. At the interface between this slice of material and the uniform field outside, compatibility is enforced by (4) and (5), while equilibrium is enforced by (6) and (7).

It is noted that the cell sides AD and BC need not be parallel with the x^2-axis in the initial configuration, as shown in Fig. 1. All equations are valid for other orientations too, e.g. for cell sides normal to the void sheet. The cells shown in Fig. 1 have the advantage that the sides remain parallel to the x^2-axis in regions where the far field is dominant.

The cell model analysis is based on a Lagrangian formulation of the field equations, using the Cartesian x^i coordinate system as reference. The Lagrangian strains are given by

$$\eta_{ij} = \tfrac{1}{2}(u_{i,j} + u_{j,i} + u_{,i}^k u_{k,j}) \tag{16}$$

where $(\ )_{,j}$ denotes covariant differentiation in the reference configuration. The contravariant components τ^{ij} of the Kirchhoff stress tensor on the deformed base vectors are related to the Cauchy stress tensor σ^{ij} by

$$\tau^{ij} = \sqrt{G/g}\,\sigma^{ij} \tag{17}$$

where g_{ij} and G_{ij} are the metric tensors in the reference configuration and the current configuration, respectively, with determinants g and G. The equilibrium equations inside the cell are expressed in terms of the principle of virtual work.

The ductile material behaviour is represented by J_2-flow theory, using the finite strain generalization discussed by Hutchinson (1973). The incremental stress–strain relationship is of the form $\dot{\tau}^{ij} = L^{ijkl}\dot{\eta}_{kl}$, with the tensor of instantaneous moduli given by

$$L^{ijkl} = \frac{E}{1+\nu}\left\{\frac{1}{2}(G^{ik}G^{jl}+G^{il}G^{jk})+\frac{\nu}{1-2\nu}G^{ij}G^{kl}-\beta\frac{3/2(E/E_t-1)}{E/E_t-(1-2\nu)/3}\frac{s^{ij}s^{kl}}{\sigma_e^2}\right\}$$
$$-\frac{1}{2}(G^{ik}\tau^{jl}+G^{jk}\tau^{il}+G^{il}\tau^{jk}+G^{jl}\tau^{ik}). \quad (18)$$

Here, $\sigma_e = (3s_{ij}s^{ij}/2)^{1/2}$ is the effective Mises stress, with $s^{ij} = \tau^{ij}-G^{ij}\tau_k^k/3$, the value of β is 1 or 0 for plastic yielding or elastic unloading, respectively, E is Young's modulus, ν is Poisson's ratio, and E_t is the slope of the true stress vs natural strain curve at the stress level σ_e. The uniaxial stress–strain behaviour is represented by

$$\varepsilon = \begin{cases} \dfrac{\sigma}{E}, & \text{for} \quad \sigma \leqslant \sigma_y \\ \dfrac{\sigma_y}{E}\left(\dfrac{\sigma}{\sigma_y}\right)^n, & \text{for} \quad \sigma > \sigma_y \end{cases} \quad (19)$$

where σ_y is the uniaxial yield stress, and n is the strain hardening exponent.

3. SIMPLE LOCALIZATION ANALYSIS

Localization induced by a sheet of voids as that shown in Fig. 1 can also be analysed by application of a porous material model. Then the void sheet is represented as a slice of material with uniform void volume fraction f^h, while there are no voids outside the band, $f^0 \equiv 0$.

The field quantities outside the band are identical to those of the uniform far field considered in Section 2, specified by the external loading. Then, with the initial angle of inclination ψ_0 of the band the current angle of inclination is still given by (1). The field quantities inside and outside the band, denoted by $(\ )^h$ and $(\ )^0$, respectively, have to satisfy compatibility and equilibrium over the band interface (see Fig. 2). In the Cartesian reference coordinate system compatibility requires continuity of the tangential derivatives of the displacement components u_i over the interface. Thus, the displacement gradients inside the band can be expressed by

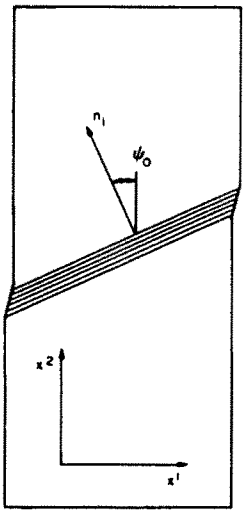

Fig. 2. Shear band in a homogeneously strained solid.

$$u_{i,I}^{b} = u_{i,I}^{0} + c_i n_I \tag{20}$$

where n_I is the unit normal in the reference state, and c_i are parameters to be determined. Equilibrium requires balance of the nominal tractions on each side of the interface

$$(T^i)^b = (T^i)^0. \tag{21}$$

A set of incremental equations for c_i are obtained by substituting the incremental constitutive relations for the porous ductile material into the incremental form of (21), using (20) to express the strain increments inside the band. From these incremental algebraic equations for c_i the onset of localization is determined as the point where elastic unloading takes place outside the band.

The porous ductile material model proposed by Gurson (1977) makes use of an approximate yield condition of the form $\Phi(\sigma^{ij}, \sigma_M, f) = 0$, where σ^{ij} is the average macroscopic Cauchy stress tensor, σ_M is an equivalent tensile flow stress representing the actual microscopic stress state in the matrix material, and f is the current void volume fraction. An approximate yield condition derived on the basis of a spherical model problem is of the form

$$\Phi = \frac{\sigma_e^2}{\sigma_M^2} + 2q_1 f \cosh\left(\frac{\sigma_k^k}{2\sigma_M}\right) - (1 + (q_1 f))^2 = 0 \tag{22}$$

where $\sigma_e^2 = (3s_{ij}s^{ij}/2)^{1/2}$ is the macroscopic effective Mises stress, defined in terms of the stress deviator $s^{ij} = \sigma^{ij} - G^{ij}\sigma_k^k/3$. The yield condition proposed by Gurson (1977) has $q_1 = 1$ in (22); but it was found by Tvergaard (1981, 1982) that using $q_1 \simeq 1.5$ gives considerably improved agreement with detailed numerical studies for periodically distributed circular cylindrical voids in elastic plastic solids (more discussion of the most appropriate q_1-value is given by Tvergaard, 1989).

The plastic part of the macroscopic strain-rate for the porous ductile material is taken to be given by

$$\dot{\eta}_{ij}^{p} = \Lambda \frac{\partial \Phi}{\partial \sigma^{ij}} \tag{23}$$

since normality of the plastic flow rule for the matrix material implies macroscopic normality (Gurson, 1977). Furthermore, defining the microscopic effective plastic strain ε_M^p in terms of the uniaxial stress–strain relation for the matrix material, $\dot{\varepsilon}_M^p = (1/E_t - 1/E)\dot{\sigma}_M$, and assuming an equivalent plastic work expression, $\sigma^{ij}\dot{\eta}_{ij}^p = (1-f)\sigma_M\dot{\varepsilon}_M^p$, the rate of change of the matrix flow stress is

$$\dot{\sigma}_M = \frac{EE_t}{E - E_t}\frac{\sigma^{ij}\dot{\eta}_{ij}^p}{(1-f)\sigma_M}. \tag{24}$$

Since the matrix material is plastically incompressible, the rate of growth of the void volume fraction is

$$\dot{f} = (1-f)G^{ij}\dot{\eta}_{ij}^p. \tag{25}$$

The value of the parameter Λ in (23) is determined from the consistency condition, $\dot{\Phi} = 0$, using (24) and (25). The result is

$$\dot{\eta}_{ij}^p = \frac{1}{H} m_{ij} m_{kl} \overset{\nabla}{\sigma}{}^{kl} \tag{26}$$

where $\overset{\nabla}{\sigma}{}^{kl}$ is the Jaumann rate of Cauchy stress and

$$m_{ij} = \frac{3}{2}\frac{s_{ij}}{\sigma_M} + \varkappa G_{ij}, \qquad \varkappa = \frac{f}{2} q_1 \sinh\left(\frac{\sigma_k^k}{2\sigma_M}\right) \tag{27}$$

$$H = \frac{\sigma_M}{2}\left[-3\varkappa(1-f)\frac{\partial\Phi}{\partial f} - \frac{\partial\Phi}{\partial\sigma_M}\frac{EE_t}{E-E_t}\frac{1}{1-f}\left(\frac{\sigma_e^2}{\sigma_M^2} + \varkappa\frac{\sigma_k^k}{\sigma_M}\right)\right]. \tag{28}$$

Plastic yielding initiates when $\Phi = 0$, and continued plastic loading requires $\Phi = 0$ and $m_{kl}\mathring{\sigma}^{kl}/H \geqslant 0$. Finally, the incremental stress–strain relationship to be used in the incremental form of (21) is obtained by taking the total strain rate to be the sum of the elastic and plastic parts, and inverting the resulting expression (see Needleman and Rice, 1978; Tvergaard, 1989).

It is noted that often nucleation of new voids is included in the porous ductile material model, by adding an extra term in (25). Furthermore, (22) can be modified to better model void coalescence at relatively large void volume fractions. However, in the present paper neither nucleation nor coalescence will be considered.

4. NUMERICAL SOLUTION PROCEDURE

The model problem illustrated in Fig. 1 is specified by a number of conditions (1)–(12) that rely on knowing the stress state and the strain state in the uniform field far away from the void sheet. This far field solution is here taken to satisfy the relation

$$\sigma_1 = \rho\sigma_2 \tag{29}$$

where ρ is a fixed ratio between the principal true stresses. The corresponding principal logarithmic strains ε_1 and ε_2 are determined by a simple incremental solution for the constitutive law with instantaneous moduli (18), so that the variation of the quantities σ_1, ε_1 and ε_2, as functions of the major principal stress σ_2, is known *a priori*.

The field equations inside the cell ABCD in Fig. 1 are solved by using a finite element approximation of the displacement fields in the incremental principle of virtual work. An example of the mesh used is shown in Fig. 3, where each quadrilateral is built up of four linear displacement triangular elements.

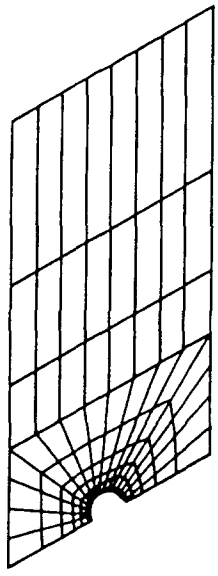

Fig. 3. Mesh used for $R_0/D_0 = 0.175$ and $\psi_0 = 30^\circ$.

A special Rayleigh–Ritz finite element method (Tvergaard, 1976) is used to implement the periodic boundary conditions. The displacements of the nodal points on the sides AD, BC and AB are chosen as parameters in the Rayleigh–Ritz solution, together with u_D^1 and u_D^2. For a small prescribed increment $\dot{\sigma}_2$ of the major tensile stress outside the band the corresponding change of the whole far field is known from the *a priori* solution, and thus the values u_A^1, u_A^2, u_B^1 and u_B^2 are directly obtained from (1)–(3). Then, the parameters in the Rayleigh–Ritz solution are determined so that the boundary conditions (4)–(12) are satisfied in addition to internal equilibrium.

Localization of plastic flow occurs when elastic unloading takes place outside the band, in the far field. In the last few increments before localization $\dot{\sigma}_2$ has to be very small to keep the incremental elongation $\dot{u}_D^2$ of the cell at a reasonable level. In these increments $\dot{u}_D^2$ is prescribed, with a reasonable estimate of $\dot{\sigma}_2$ used in (1)–(3), and elastic unloading outside the band is taken to be defined by $\dot{\sigma}_2 < 0$ according to the integral (6) along the edge of the cell. When the computation is continued beyond localization, $\dot{u}_D^2$ is also taken to be prescribed, but here the small reductions of ε_1 and ε_2 during elastic unloading are neglected in (1)–(3).

It is noted that, as a check, the same computation has been carried out with a regular mesh inside the region ABCD, representing the case where there are no voids. For this case it was confirmed that the uniform solution inside the cell, resulting from (1)–(12), remained identical to the far field.

5. RESULTS

The material to be analysed here is taken to have the initial yield stress $\sigma_y/E = 0.002$, the strain hardening exponent $n = 10$, and Poisson's ratio $\nu = 0.3$. The initial dimensions of the cell analysed (see Figs 1 and 3) are specified by $B_0/A_0 = 4$, and in most of the cases considered the material far from the void sheet is subjected to uniaxial plane strain tension, as specified by $\rho = 0$ in (29).

Figure 4 shows deformed meshes and contours of constant maximum principal logarithmic strain at two stages of deformation in a case where the initial void size is specified by $R_0/D_0 = 0.125$, and the initial angle of inclination of the void sheet is $\psi_0 = 30°$. At the first stage (Fig. 4a) the major principal logarithmic strain in the far field is $\varepsilon_2 = 0.033$, finite strains have started to occur near the void, and the void has grown a little to $V/V_0 = 1.28$, where V and V_0 are the current void volume and the initial void volume, respectively.

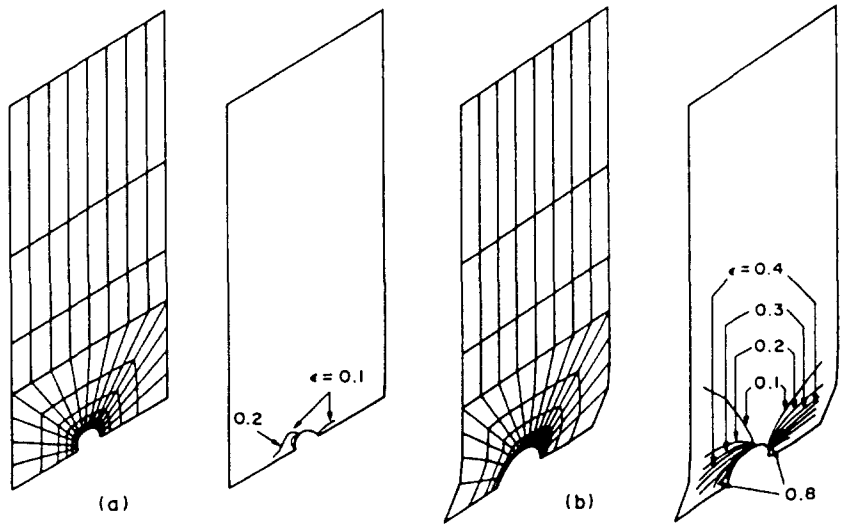

Fig. 4. Deformed meshes and contours of constant maximum principal logarithmic strain for $R_0/D_0 = 0.125$ and $\psi_0 = 30°$. (a) At $\varepsilon_2 = 0.033$, (b) after localization, which occurs at $\varepsilon_2 = 0.083$.

Localization of plastic flow occurs at the critical strain $\varepsilon_2^c = 0.083$ (in the far field), where elastic unloading takes place in most of the region analysed, away from the void. The second stage (Fig. 4b) is well beyond the onset of localization, with $V/V_0 = 3.36$ and very high level of straining in the material near the void. Both the strain contours and the deformed mesh show that the high localized deformations occur in a rather narrow band, which is not much wider than the current void dimension. In the top part of the region analysed the stress and strain fields remain nearly uniform throughout the deformation, at levels agreeing very well with the specificed far field, as expected.

Figure 5 shows similar results for a larger initial void, specified by $R_0/D_0 = 0.25$, again with $\psi_0 = 30^\circ$ and $\rho = 0$. The far field strains at the first two stages are $\varepsilon_2 = 0.0036$ and $\varepsilon_2 = 0.0106$, respectively, while the last stage (Fig. 5c) is way beyond localization, which occurs at $\varepsilon_2^c = 0.0118$. Thus, localization occurs soon after the stage in Fig. 5b; but it is seen that the level of straining inside the band is much higher in Fig. 5c. As in Fig. 4 the width of the band containing the highly strained material appears to be a little wider than the current void dimension.

Figure 6 shows plots of the localization strain ε_2^c vs the initial angle of inclination of the void sheet. The minima of the curves determine the most critical orientations of the void sheets. Results of 12 different numerical analyses are shown, covering three different values of R_0/D_0, 0.125, 0.175 and 0.25, and including the results corresponding to Figs 4 and 5. Localization results obtained by the simple analysis (20), (21) are also shown in Fig. 6, thus using the porous material model (22)–(28), with $q_1 = 1.5$, to represent the void-sheet. With no voids outside the band, $f^0 \equiv 0$, the void-sheet is here represented by considering initial void volume fractions inside the band ranging from $f_1^b = 0.03$ to $f_1^b = 0.08$. Since the strain fields outside the band used for the simple analysis are identical to the far fields used in the full numerical model problem, the current angle of inclination ψ at a given strain level is the same for both models, as specified by (1).

It is seen in Fig. 6 that the general shapes of the curves found by the cell model analysis are in good agreement with those given by the simple shear band analysis. However, the minima of the curves predicted by the cell model analysis occur at somewhat smaller values of the initial angle of inclination ψ_0 of the void sheet; about 5° smaller than the values found by the simple analysis. Therefore, also the current angle of inclination at the onset of localization is smaller for the cell model analysis [see (1)].

Interpolation between the curves for various values of f_1^b in Fig. 6 can be used to estimate the initial void volume fraction that gives a localization strain corresponding to that found for a given value of R_0/D_0. According to Fig. 6 the minimum localization strains obtained for the values 0.125, 0.175 and 0.25 of R_0/D_0 are also approximately obtained for

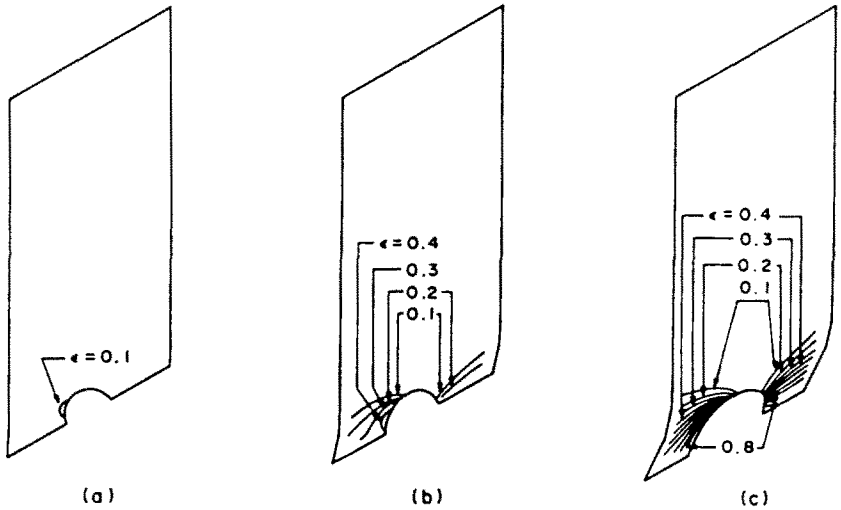

Fig. 5. Contours of constant maximum principal logarithmic strain for $R_0/D_0 = 0.25$ and $\psi_0 = 30^\circ$. (a) At $\varepsilon_2 = 0.0036$, (b) at $\varepsilon_2 = 0.0106$, (c) after localization, which occurs at $\varepsilon_2^c = 0.0118$.

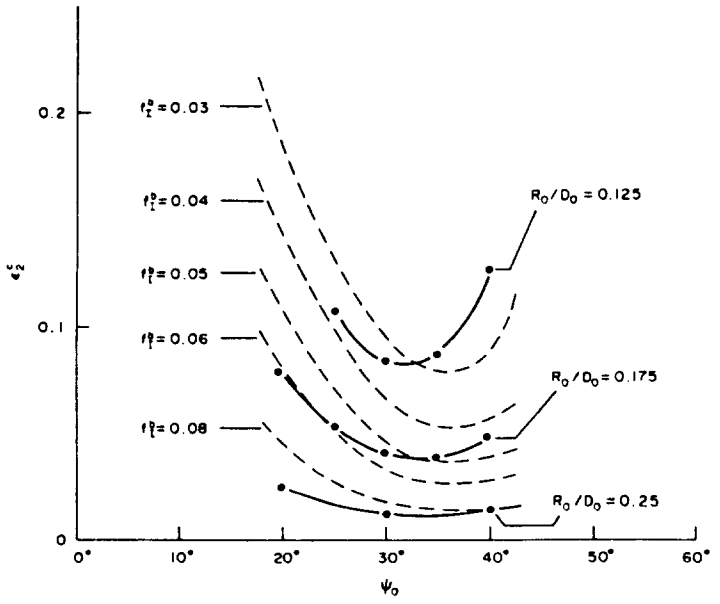

Fig. 6. Localization strain vs initial angle of inclination of the void sheet. Predictions based on simple shear band model are shown for comparison, for various initial void volume fractions f_I^0, and $q_1 = 1.5$.

the initial void volume fractions 0.029, 0.049 and 0.084, respectively, in the simple shear band analysis.

Representing a row of voids as that shown in Fig. 1 in terms of a porous ductile material model makes it necessary to estimate the appropriate void volume fraction in the void sheet; but this requires knowledge of the width of the porous slice of material. If the initial band width $2W_0$ is known, together with the void spacing $2D_0$ and the radius R_0, the void volume fraction inside the band can be calculated directly. The curves in Fig. 7

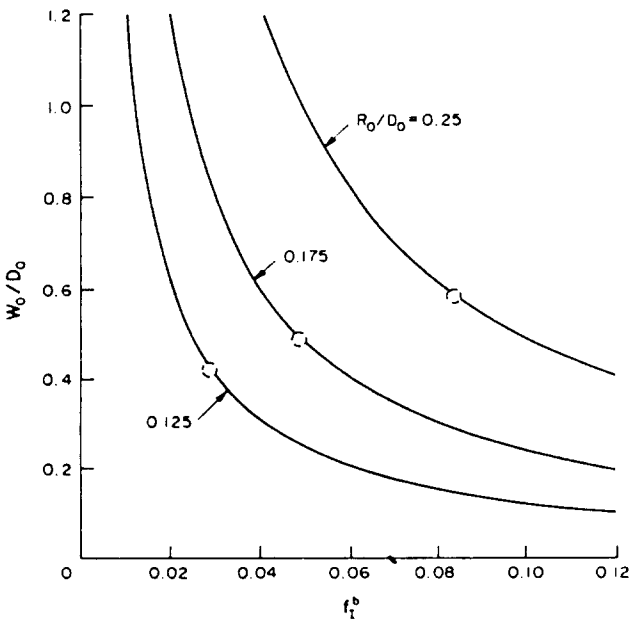

Fig. 7. Corresponding values of initial band width $2W_0$ and void volume fraction f_I^0, for various values of R_0/D_0. The values found in Fig. 6 are indicated by dashed circles.

show corresponding values of the ratio W_0/D_0 and the void volume fraction f_1^h, for the three different values 0.125, 0.175 and 0.25 of the ratio R_0/D_0. The values of f_1^h that give approximately the same localization strains as those found in Fig. 6 by the full numerical analysis (see discussion above) are indicated on the curves as dashed circles. These three points in Fig. 6, which rely on a comparison of localization predictions, provide an estimate of the appropriate band width that should be used to calculate "the void volume fraction in the void-sheet". It is seen that the appropriate band width is of the order of half the void spacing, somewhat increasing with increasing void size relative to the void spacing. In fact, the expression

$$W_0/D_0 \simeq 0.3 + R_0/D_0 \tag{30}$$

gives a rather good representation of the band widths specified by the three points in Fig. 7.

The effect of stress triaxiality on the localization predictions has been studied by considering far fields with a constant ratio $\rho = \sigma_1/\sigma_2$ between the principal true stresses [see (29)]. Here, for simplicity the initial angle of inclination of the void sheet is taken to be $\psi_0 = 30^\circ$ in all cases, and only the intermediate void size $R_0/D_0 = 0.175$ is considered. In Fig. 8 the predictions based on the simple shear band analysis and the porous material model with $f_1^h = 0.06$ and $\psi_0 = 30^\circ$ are included as a reference curve. For $\rho = 0$ (uniaxial plane strain tension) it is already known from Fig. 6 that this reference curve is a little below the prediction based on the cell model analysis.

Figure 8 shows that the localization strain is strongly dependent on the stress state. For $\rho > 0$ the increased hydrostatic tension gives rapid void growth, which results in much earlier localization, while the opposite effect is found for $\rho < 0$. For positive values of ρ there is reasonable agreement between the predictions of the cell model analysis and those of the simple shear band analysis. However, as ρ becomes negative there is an increasing delay of the cell model localization predictions, relative to the simple model. In fact, a cell model calculation carried out for $\rho = -0.5$ was stopped at $\varepsilon_2 = 0.234$, prior to any localization, when the void volume was significantly reduced and the void had been flattened out so that contact between void surfaces would have to be accounted for in a continued computation. Based on the results of Fleck *et al.* (1988) for voids in pure shear fields, or shear fields with superposed tension, such void closure would be expected for sufficiently

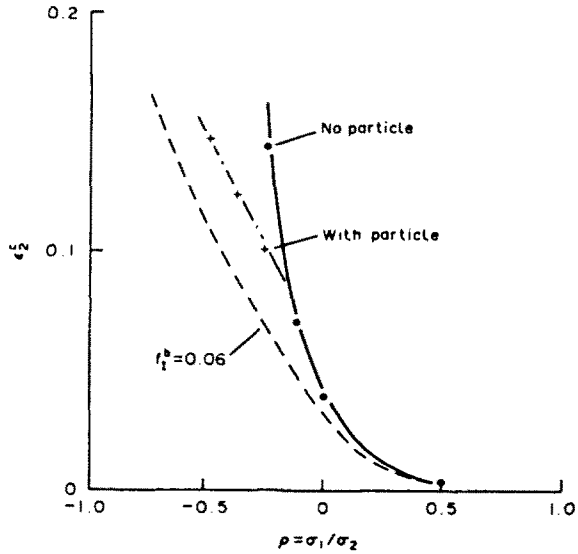

Fig. 8. Localization strain vs principal true stress ratio, for $R_0/D_0 = 0.175$ and $\psi_0 = 30^\circ$. Predictions based on simple shear band model for $f_1^h = 0.06$ are shown for comparison.

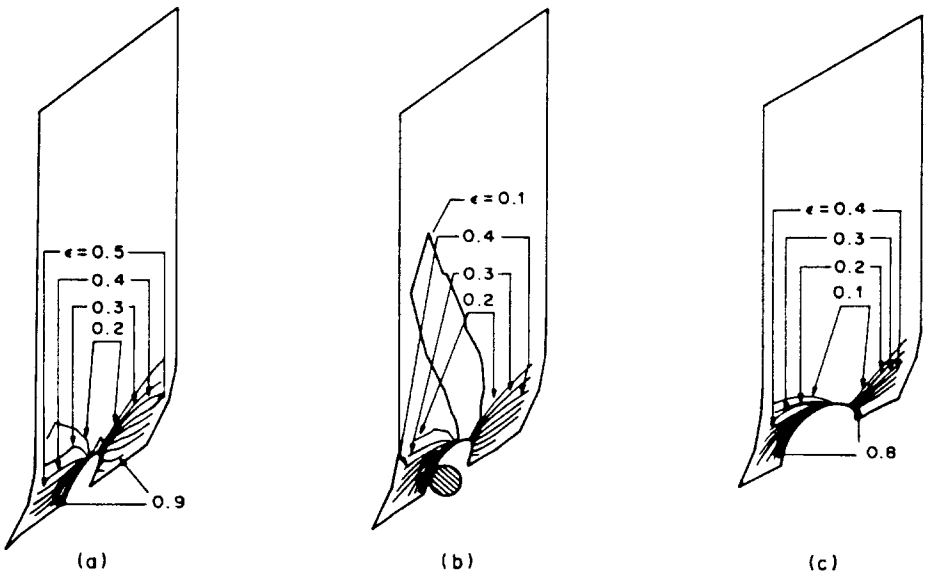

Fig. 9. Contours of constant maximum principal logarithmic strain at a stage beyond the onset of localization, for $R_0/D_0 = 0.175$, $\psi_0 = 30^\circ$ and a principal stress ratio ρ. (a) $\rho = -0.25$ with no particle, (b) $\rho = -0.25$ with rigid particle inside void, (c) $\rho = 0.25$.

low values of ρ; but this flattening and closure of voids is not accounted for in the porous ductile material model (22) (28).

When the void is nucleated from a particle, by debonding of the particle matrix interface at some stage, contact between particle and void surface can have a significant influence on the subsequent behaviour, as has been found by Fleck *et al.* (1988). Assuming here that the void nucleates at zero strain, from a rigid, circular cylindrical particle, the effect of subsequent sliding contact between particle and void surface is expressed by (15). This contact becomes active in a range of negative ρ values, where the voids would like to flatten out and even close. In this range the particle pressure on the void surface results in (additional) void growth. It is seen in Fig. 8 that the effect of the particles promotes localization significantly.

The effect of a particle was also accounted for in the computation of the localization strain plotted for $\rho = -0.125$ in Fig. 8, and there was sliding contact between the particle and the void surface. However, in this case the void surface pulled away from the particle somewhat before the onset of localization.

Figure 9 shows contours of constant maximum principal logarithmic strain for three of the computations plotted into Fig. 8. Figure 9a and b correspond to $\rho = -0.25$, without particle and with particle, respectively, while Fig. 9c corresponds to $\rho = 0.25$. In all three cases the stage shown is well beyond the onset of localization, and the width of the highly strained band of material is of the order of the current void dimension. The current values of V/V_0 in the three cases are 1.85, 2.90 and 4.28, respectively. Thus, in Fig. 9a the value of ρ is still so large that the void grows; but the smaller axis of the oval void in Fig. 9a is not as large as the particle, and therefore the particle in Fig. 9b has given rise to more void growth and earlier localization. The significant void growth due to superposed hydrostatic tension in Fig. 9c is the reason for the early localization predicted in this case.

An analysis has also been carried out for which the particle is initially fully bonded [described by (14)], but nucleates later at $\varepsilon_2 = 0.1$. The case considered has $\rho = 0$, $R_0/D_0 = 0.175$ and $\psi_0 = 30^\circ$, no nucleation occurs well after the onset of localization in the absence of particles (see Figs 6 and 8). Nucleation is modelled by releasing the nodes on the particle–matrix interface and stepping down the node forces in a number of subsequent increments. In the case analysed, elastic unloading of the far fields occurs immediately when nucleation starts, and during the subsequent localized straining in a band of material along the void-sheet the macroscopic stress level prior to nucleation is never reached again.

Thus, localization is simultaneous with nucleation in this case, as would be expected when nucleation occurs much later than the localization predicted in the absence of particles. Clearly, before nucleation the onset of localization is prevented by the particle stiffening effect.

6. DISCUSSION

Previous analyses of the effect of a void sheet on the onset of plastic flow localization have relied on the application of porous ductile material models. The micromechanical analyses in the present paper are a first attempt on a full solution for a row of voids, taking into account the detailed stress and strain fields around each void, the changes of the void shape, and the interaction between neighbouring voids. It is found that localization of plastic flow is actually predicted in a narrow zone around the void sheet. Furthermore, for a given initial geometry of the void sheet the smallest critical localization strain is found for a certain critical angle of inclination of the void sheet, as expected. The current angle of inclination at first critical localization is found to be around 37° in the cases of uniaxial plane strain tension considered here; somewhat smaller than the values predicted by porous ductile material models.

The choice of material model for the matrix material would have a strong effect on localization predictions. Here, strain hardening J_2 flow theory is used, so it is known beforehand that all matrix material will remain in the elliptic range, and that even inhomogeneities will not give shear localization in the matrix (Rice, 1977; Hutchinson and Tvergaard, 1981). Therefore, in the cases analysed, localization of plastic flow can only occur as a result of the voids. The same classical plasticity model was used for the matrix material in previous micromechanical studies of localization (Tvergaard, 1981, 1982), and is also the basis of the porous ductile material model (22) (28).

The void volume fraction distributions in a material containing a single layer of voids are not well defined, and therefore comparison with localization predictions based on porous ductile material models is difficult. In fact, the present micromechanical studies can be directly used to calibrate the porous material model, i.e. determine the appropriate void volume fraction for representing a single layer of voids as a porous slice of material. According to Figs 6 and 7 the appropriate band width used to calculate the void volume fraction should be about half the void spacing, somewhat larger for larger voids relative to the spacing. A somewhat different interpretation is obtained from the contour plots in Figs 4, 5 and 9, which show that the width of the highly deformed band of material is of the order of the largest dimension of the deformed void. It is noted that these predictions are entirely based on a void-sheet made up of a single row of circular cylindrical voids; but it is expected that a sheet of periodically distributed spherical voids would behave in about the same way. Clearly, a micromechanical analysis accounting for spherical voids inside the band would have to be a three-dimensional analog of the cell model analyses carried out here.

The appropriate width and void volume fraction of a porous zone used to represent a single layer of voids has been discussed in some detail by Becker *et al.* (1989), who studied ductile crack growth in an Al–Li alloy for which void nucleating particles appear predominantly at the grain boundaries. Based on Tvergaard's (1982) comparison of numerical results for arrays of spherical voids with the porous material model it was argued that the most realistic width of the grain boundary porous zone, for use in converting the area fraction of voids to a volume fraction, is of the order of the void spacing. It was emphasized by Becker *et al.* (1989) that the estimate based on these comparisons would only apply when the maximum principal stress direction is normal to the grain boundary. Now, on the basis of the present investigation it appears that for boundaries inclined to the maximum principal stress direction the width of the grain boundary porous zone should be chosen somewhat smaller, of the order of half the void spacing.

The effect of the inclusion remaining inside the void after nucleation is usually neglected in porous ductile material models. This is quite reasonable in a large range of stress states, where the void expands to dimensions larger than the particle. However, in the range of

rather low hydrostatic tension the voids tend to flatten out, so that their minimum dimension does not allow for the presence of the particle. For such cases Fleck *et al.* (1988) have analysed the influence of sliding contact between the particle and the void surface and found that the effect of the particles can significantly add to the void growth, or even give void growth where there would otherwise have been void closure. The present micromechanical studies show (Fig. 8) that also the onset of plastic flow localization is strongly affected by the particles. In the absence of particles, at low levels of triaxial tension, the voids close up, and no localization is predicted, whereas the presence of particles enforces a material softening that finally results in localization.

REFERENCES

Becker, R., Needleman, A., Suresh, S., Tvergaard, V. and Vasudevan, A. K. (1989). An analysis of ductile failure by grain boundary void growth. *Acta Metal.* **37**, 99–120.

Fleck, N. A., Hutchinson, J. W. and Tvergaard, V. (1988). Softening by void nucleation and growth in tension and shear. Harvard University, Division of Applied Science, MECH-123.

Gurson, A. L. (1977). Continuum theory of ductile rupture by void nucleation and growth—I. Yield criteria and flow rule for porous ductile media. *J. Engng. Mater. Technol.* **99**, 2–15.

Hutchinson, J. W. (1973). Finite strain analysis of elastic–plastic solids and structures. In *Numerical Solution of Nonlinear Structural Problems* (Edited by R. F. Hartung), p. 17. ASME, New York.

Hutchinson, J. W. and Tvergaard, V. (1981). Shear band formation in plane strain. *Int. J. Solids Structures* **17**, 451–470.

Koplik, J. and Needleman, A. (1987). Void growth and coalescence in porous plastic solids. Brown University, Division of Engineering.

Mear, M. E. and Hutchinson, J. W. (1985). Influence of yield surface curvature on flow localization in dilatant plasticity. *Mech. Mater.* **4**, 395–407.

Needleman, A. and Rice, J. R. (1978). Limits to ductility set by plastic flow localization. In *Mechanics of Sheet Metal Forming* (Edited by D. P. Koistinen *et al.*), pp. 237–267. Plenum, London–New York.

Rice, J. R. (1977). The localization of plastic deformation. In *Theoretical and Applied Mechanics* (Edited by W. T. Koiter), pp. 207–220. North Holland, Amsterdam.

Saje, M., Pan, J. and Needleman, A. (1982). Void nucleation effects on shear localization in porous plastic solid. *Int. J. Fract.* **19**, 163–182.

Tvergaard, V. (1976). Effect of thickness inhomogeneities in internally pressurized elastic–plastic spherical shells. *J. Mech. Phys. Solids* **24**, 291–304.

Tvergaard, V. (1981). Influence of voids on shear band instabilities under plane strain conditions. *Int. J. Fract.* **17**, 389–407.

Tvergaard, V. (1982). On localization in ductile materials containing spherical voids. *Int. J. Fract.* **18**, 237–252.

Tvergaard, V. (1987). Effect of yield surface curvature and void nucleation on plastic flow localization. *J. Mech. Phys. Solids* **35**, 43–60.

Tvergaard, V. (1988). 3D-analysis of localization failure in a ductile material containing two size-scales of spherical particles. *Engng. Fract. Mech.* **31**, 421–436.

Tvergaard, V. (1989). Material failure by void growth to coalescence. *Adv. Appl. Mech.* (to appear).

Yamamoto, H. (1978). Conditions for shear localization in the ductile fracture of void-containing materials. *Int. J. Fract.* **14**, 347–365.